Conference on Modelling Fluid Flow (CMFF'25)
The 19th International Conference on Fluid Flow Technologies
Budapest, Hungary, August 26 - August 29, 2025

INFLUENCE OF PACKING DENSITY ON THE CALCINATION PROCESS FOR LIME PRODUCTION: A DEM-CFD STUDY

Rezvan ABDI[1,2], Bo JAEGER[2], Torben BERGOLD[2], Enric ILLANA[2], Martin SCHIEMANN[2] and Viktor SCHERER[2]

[1]Corresponding Author. Tel.: +49 234 / 32-17986. E-mail: Abdi@leat.rub.de
[2]Institute of Energy Plant Technology, Ruhr-University Bochum, Universitätsstraße 150, 44780 Bochum, Germany.

ABSTRACT

To model the calcination of limestone in a moving particle bed, a radiation model based on the Discrete Ordinates Method (DOM) is incorporated into Computational Fluid Dynamics (CFD) and coupled with the Discrete Element Method (DEM). By accounting for local porosity, the radiation model adjusts the net radiative heat flux over the packing density accordingly.

The endothermic calcination reaction converts limestone ($CaCO_3$) into quicklime (CaO). The paper evaluates radiation penetration, temperature distributions, calcination degree, and CO_2 mass fraction in a system where limestone particles are heated by a gas in crossflow and a radiative enclosure. In addition to convection and radiation, conductive heat transfer among particles is accounted for. Three different packing conditions—dilute, moderate, and dense—are investigated.

Results highlight the significant role of radiation in driving the calcination process, as well as the dependence of radiation—and consequently calcination—on packing density. The study shows that the calcination degree decreases with increasing packing density. The simulation results yield average calcination degrees of 98%, 80%, and 60% for particles at the outlet in the dilute, moderate, and dense configurations, respectively.

Keywords: Lime Production, DEM, CFD, Calcination, DOM Radiation, AVM

NOMENCLATURE

a	[1 m^{-1}]	absorption coefficient
E_a	[kJ mol^{-1}]	activation energy
$k'_{r,s}$	[m s^{-1}]	reaction rate
I	[W m^{-2} sr^{-1}]	radiative intensity
rp_s	[-]	reaction progress
V_m	[m^3 mol^{-1}]	solid molar volumes
Y_{CO_2}	[-]	CO_2 mass fraction

Subscripts and Superscripts

CV	control volume
eff	effective
f	fluid
$Proj$	projected

1. INTRODUCTION

Quicklime (CaO) plays a crucial role in various industrial applications, including steel manufacturing, wastewater treatment and flue gas desulfurization. Its production is based on the thermal decomposition of limestone ($CaCO_3$) through calcination, which is commonly carried out in shaft kilns. Calcination is a thermally driven endothermic reaction, which requires 178 kJ/mol, that decomposes calcium carbonate into calcium oxide and carbon dioxide ($CaCO_3(s) \rightarrow CaO(s) + CO_2(g)$).

In recent years, significant research efforts have been dedicated to modelling and simulating the internal environment of lime shaft kilns to gain a clearer understanding of the complex mechanisms governing thermochemistry and material transport. Conventional methods often utilize one-dimensional (1D) heat and mass balance techniques or Computational Fluid Dynamics (CFD) models that tend to simplify the representation of solid particles. A more advanced approach integrates a particle-scale calcination model at a sub-grid resolution to offer deeper insights into shaft kiln behaviour [1].

To achieve a more realistic description of the calcination phenomena, researchers have investigated the application of the Discrete Element Method (DEM). This approach solves the motion and interactions among individual particles according to Newton's laws of motion [2]. DEM is a highly effective tool for studying the dynamics of particle-based systems due to its ability to easily access information at the individual particle level [3]. It enables a more precise description of the limestone bed's granular structure within the kiln. When

coupled with CFD, a comprehensive analysis of thermochemical processes by modelling both particle dynamics and gas-phase interactions is feasible. However, due to the computational challenges posed by the large number of particles in industrial-scale kilns, DEM-based simulations remain relatively scarce.

Several studies have successfully integrated DEM and CFD to investigate different kiln configurations, including single-shaft kilns [4-5] and regenerative two-shaft kilns [6]. Additionally, simulations of oxyfuel calcination have been conducted in [7].

Intra-particle heat and mass transfer adds another layer of complexity to kiln modelling. The particles in lime production are thermally thick and hence gradients of temperature and species must be resolved in the interior of the particle. In previous work [1], the particles are modelled as spheres and the calcination process is simulated using a shrinking core model, where the outer layer of the particle reacts first, gradually transitioning to the core as the reaction progresses. In another approach [6-7], thermally thick particles are modelled by discretizing the particle into concentric shells. Each shell is assumed to have a uniform temperature and heat conduction and mass transfer are solved radially through the particle. The same approach is used in this study.

A notable gap in current research is the absence of detailed 3D DEM-CFD studies for lime production that accurately incorporate radiation effects using the Discrete Ordinates Method (DOM). To the best of the authors' knowledge, this aspect has not been extensively explored in the literature. This study utilizes the DOM method, which is particularly effective for handling directional variability in radiation. This technique discretizes the radiation field into a set of fixed directions in the Cartesian system, solving the Radiative Transfer Equation (RTE) for each direction [8].

In DEM-CFD simulations involving large numbers of particles, the bulk can be efficiently represented within the Eulerian CFD framework using the Average Volume Method (AVM). Instead of individually resolving the particles and the voids between them [2], this method represents particles through a porosity field and all relevant properties are volume-averaged. The transfer of mass, energy, and species is computed for each particle and then distributed across the CFD domain accordingly. As a result, the precise shape of individual particles is not resolved during the CFD simulation.

In this study, to enable efficient computation, AVM is utilized by deriving a time-resolved porosity distribution from DEM. This strategy allows for multiple particles to be contained within a single CFD control volume, enabling the modelling of solid-fluid interactions at subgrid interfaces. The AVM model used here considers radiation shadowing between 'particle layers' in adjacent fluid cells [8].

A major contribution of this study is the detailed investigation of heat transfer mechanisms—including convection, contact conduction, and radiation—within a moving packed particle system. By adjusting absorption and emission coefficients in the DOM for varying packing densities, the study ensures accurate distribution of radiative heat in fluid cells. The accuracy of this adjustment is validated through comparison with experimental and numerical data, which were presented in our previous publication [8]. Additionally, for cases where only the overall effect of radiation shadowing is of interest, this approach may eliminate the necessity of particle-particle radiation modelling. This study is an extension of our previous work [8], in which calcination was not considered, and the results were obtained at much smaller particle residence times.

The proposed model has been integrated into an in-house DEM software, developed within the Bulk-Reaction research centre [9], supported by funding from the German Research Foundation. The DEM software is coupled with OpenFOAM [10] to solve for the energy, species, and mass transport in the gas phase. Section 2 introduces the calcination and radiation modelling approach, followed by a comparative analysis of scenarios with and without calcination in Section 3, and a summary of key findings in Section 4.

2. MODEL DESCRIPTION

2.1. Discrete Element Method (DEM)

Each particle is represented as an isotropic, homogeneous porous material. The motion of spherical limestone particles is tracked using the Discrete Element Method (DEM). For brevity, the details of the equations are referred to in [7].

2.2. Computational Fluid Dynamics (CFD)

The CFD component ensures mass, momentum and energy conservation in the fluid phase by solving the following transport equations:

$$\frac{\partial \phi \rho_f}{\partial t} + \nabla \cdot \left(\phi \rho_f \underline{u}_f\right) = S_{gas} \tag{1}$$

$$\frac{\partial (\phi \rho_f \underline{u}_f)}{\partial t} + \nabla \cdot \left(\phi \rho_f \underline{u}_f \underline{u}_f\right) = -\phi \nabla p + \phi \nabla \cdot \tau_f + \phi \rho_f \underline{g} + S_M \tag{2}$$

$$\frac{\partial (\phi \rho_f h_f)}{\partial t} + \nabla \cdot \left(\phi \rho_f \underline{u}_f h_f\right) = \nabla \cdot \left(\phi \, k_f \, \nabla T\right) + S_E \tag{3}$$

The fluid phase is characterized by its velocity $\underline{u_f}$, density ρ_f, porosity ϕ and specific enthalpy h_f. In these fluid equations, the local bed porosity (provided by the DEM model for each fluid cell) is used. S_{gas} is the mass (air and CO_2) exchanged with the solid phase. The momentum source terms include the pressure gradient ∇p, the stress tensor τ_f (assuming laminar flow), the gravitational acceleration $\underline{g}$ and the momentum exchanged with the particles S_M. In this formulation, S_M is determined using the Ergun equation [11]. Regarding the energy equation, the fluid's thermal conductivity is represented by k_f while the enthalpy exchange with the solid phase corresponds to S_E.

The transport equation for chemical species is expressed as:

$$\frac{\partial(\phi\rho_f Y_{CO_2})}{\partial t} + \nabla\cdot\left(\phi\rho_f \underline{u_f} Y_{CO_2}\right) = \nabla\cdot\left(\phi\rho_f D_{CO_2}\nabla Y_{CO_2}\right) + S_{CO_2} \quad (4)$$

The gas phase comprises the components H_2O, CO_2, N_2 and O_2. To simplify the modelling process, the species transport equation is solved only for the mass fraction Y_{CO_2}, as it significantly influences the calcination rate of lime particles. Additionally, the source term S_{CO_2} and the term including the diffusion coefficient D_{CO_2} model the release and transport of CO_2 from the particles during the calcination reaction, respectively.

2.3. Convective and Conductive Heat Transfer

The convective heat transferred, $\dot{Q}_{conv}$ [W], is given by:

$$\dot{Q}_{conv} = \alpha\, A_p \left(T_f - T_{p,surf}\right) \quad (5)$$

where T is the temperature, A_p represents the particle's surface area, and α denotes the convective heat transfer coefficient. Further details on the calculation of the α can be found in [7].

The contact heat transfer among particles is influenced by two main mechanisms: heat conduction through particle contact points and the gas layer in the vicinity of the contact points. Details of the equations can be found in Hilse et al. [12].

2.4. Radiation Model

Equation (6) provides a simplified form of the Radiative Transfer Equation (RTE), which characterizes the propagation of radiation along a specific direction $\underline{s}$ through a medium. The term $I_{(\underline{s},\underline{r})}$ denotes the radiation intensity [W/(m^{2}sr)] at position $\underline{r}$ and along direction $\underline{s}$. To determine $I_{(\underline{s},\underline{r})}$, the Discrete Ordinates Method (DOM) solves a predetermined set of RTEs. The radiation balance for an individual CFD cell results in the discretised formulation of the RTE (Eq. (7)). In addition, the net radiative heat flux to the particles within the system is expressed in Eq. (8).

$$(\nabla\cdot I)_{(\underline{s},\underline{r})}\cdot\underline{s} = -a_p\, I_{(\underline{s},\underline{r})} + \frac{E_p}{4\pi} \quad (6)$$

$$\sum_i^{N_{ray}}\sum_{face} I_{face,i}\,\underline{S_i}\,\underline{A_{face}} = -a_p\,\omega_i I_{cell,i} + \frac{E_p}{4\pi}\omega_i \quad (7)$$

$$\dot{Q}_{net\ rad.\ D-P} = \dot{Q}_{absorbed\ rad.\ p.} - \dot{Q}_{emitted\ rad.\ p.} = \epsilon_{rad,p}\phi A_p\left(\frac{G_{cell}}{4} - \sigma T_p^4\right) \quad (8)$$

where $\underline{S_i} = \underline{s_i}\omega_i$, ω_i is the discrete solid angle associated to a specific direction i, ϕ is the local bed porosity, $\epsilon_{rad,p}$ is the emissivity of the particle, G is incident radiation, σ is Stefan-Boltzmann constant. a_p is the particle absorption and E_p is the particle emission which is computed based on:

$$a_p = \frac{1}{V_{cell}}\phi\sum_{i=1}^{N}\epsilon_{rad,p}\,A_{Proj,i} \quad (9)$$

$$E_p = \frac{1}{V_{cell}}\phi\sum_{i=1}^{N}\epsilon_{rad,p}A_{p,i}\sigma\,T_{p,i}^4 \quad (10)$$

where V_{cell} is the CFD cell volume and $A_{Proj,i}$ denotes the area of the particle projected in the i-th direction.

As shown in the equations above, incorporating local bed porosity ϕ into the modelling of particle emission, absorption, and radiation propagation enables the model to account for the effects of varying packing densities. Further details on the DOM model, and its validation are available in our earlier publication [8].

2.5. Model for Intraparticle Calcination

A radially resolved model is used to track the conversion of limestone to quicklime. By discretizing a spherical particle into 40 radial control volumes (shells), the internal temperature distribution and reaction kinetics are solved. The particle's outer diameter remains constant, which is a reasonable assumption for limestone. The calcination degree is the ratio of the CO_2 released to the initial amount of CO_2 bound in $CaCO_3$.

$$D_{calcination,p} = \frac{m_{CaCO_3} - m(t)}{m_{CaCO_3} - m_{CaO}} \quad (11)$$

where m_{CaCO_3} is the initial mass of $CaCO_3$, $m(t)$ is the time-varying particle mass and m_{CaO} is the mass of CaO corresponding to fully calcined particles. The porosity of each shell, ε_s, is determined by considering the solid molar volumes V_m, the initial porosity of the limestone ε_{CaCO_3}, and reaction progress rp_s:

$$\varepsilon_s = \varepsilon_{CaCO_3} + \left(1 - \frac{V_{m,CaO}}{V_{m,CaCO_3}}\right)(1 - \varepsilon_{CaCO_3})\, rp_s \quad (12)$$

The reaction progress ranges from zero to one, indicating the extent of the calcination. It is mathematically defined as the ratio of the mass of calcium oxide ($m_{s,CaO}$) formed at any given stage to the total mass of calcium oxide that would be produced upon complete calcination:

$$rp_s = \frac{m_{s,CaO}}{(1-\varepsilon_{CaO})\, \rho_{CaO}\, V_s} \quad (13)$$

where V_s is the shell volume, ρ_{CaO} is the lime density and ε_{CaO} is the lime porosity. The porosity of lime (ε_{CaO}) is calculated from equation (13) by setting the reaction progress (rp_s) to 1, ensuring that it corresponds to the fully reacted state of the material.

At this stage, it is considered that the shell's solid temperature is in thermal equilibrium with the gas temperature within its pores, primarily due to the large surface area. It is also crucial to highlight that heat sources from convection, surface contact, and radiation are only applied to the outermost shell (control volume, CV).

$$V_s\, \rho_s c_{p,s} \frac{\partial T_s}{\partial t} = A_j k_j \nabla T_s + \dot{Q}_{conv} + \dot{Q}_{net\ rad\ D-P} + \dot{Q}_{contact} + \dot{Q}_{r,s} \quad (14)$$

Here, $c_{p,s}$ is the shell specific heat capacity, $\dot{Q}_{r,s}$ represents the heat generated by the reaction in each shell, and the subscript j denotes the boundary separating two adjacent control volumes (CVs), where interpolation based on CV values is utilized, with the exception of the area A_j. The rate of CO_2 release in each shell is obtained based on:

$$\frac{dn_{CO_2,s}}{dt} = A_{r,s}\, k'_{r,s}\left(c_{CO_2,s} - c_{CO_2,eq}\right) \quad (15)$$

where $A_{r,s}$ is the shell area of reaction and $k'_{r,s}$ is the reaction rate. The CO_2 concentration, $c_{CO_2,s}$, is:

$$c_{CO_2,s} = \frac{\rho_{gas,s} \cdot Y_{CO_2,s}}{M_{CO_2}} \quad (16)$$

The equilibrium CO_2 concentration, $c_{CO2,eq}$, is also temperature-dependent:

$$c_{CO_2,eq} = \frac{1}{R_m T_s}\left(101325 \cdot \exp\left(17.74 - 0.00108\, T_s + 0.332 \ln(T_s) - \frac{22020}{T_s}\right)\right) \quad (17)$$

where R_m is the universal gas constant. The associated reaction rate is defined by an Arrhenius-type expression:

$$k'_{r,s} = K_0\, T_s^{\,b}\, e^{-\frac{E_a}{R_m T_s}}\, K_{T,c} \quad (18)$$

where the activation energy is $E_a = 33.474$ [kJ/mol], the temperature exponent is $b = 1$ and the pre-exponential factor is $K_0 = 10^{-4}$ [$\frac{\mathrm{m}}{\mathrm{sK}}$]. The term $K_{T,c}$ represents a correction factor, as described in reference [7].

Hence, higher T accelerates reaction rate via the Arrhenius term and higher CO_2 concentrations slows down calcination by reducing the driving force for CO_2 to diffuse from within the particle and by shifting the equilibrium toward $CaCO_3$ formation.
Assuming that air and carbon dioxide are the only gaseous components present inside the particle, the transport equations, in their spatially discretized form are then expressed as:

$$\varepsilon_s\, V_s \frac{\partial \rho_{gas,s}}{\partial t} = -\sum(\rho_{gas,j}\ A_j\, \underline{v}'_j) + M_{CO_2} \frac{dn_{CO_2,s}}{dt} + S_{gas} \quad (19)$$

$$\varepsilon_s\, V_s \frac{\partial\left(\rho_{gas,s}\, Y_{CO_2,s}\right)}{\partial t} = -\sum\left(\varepsilon_s \rho_{gas,j}\, A_j \left(\underline{v}'_j\, Y_{CO_2,s} - D_{CO_2}\, \nabla Y_{CO_2,s}\right)\right) + M_{CO_2} \frac{dn_{CO_2,s}}{dt} + S_{CO_2} \quad (20)$$

where M_{CO_2} is the molecular weight of CO_2, $n_{CO_2,s}$ is the number of moles of CO_2 in shell s. The advection velocity $\underline{v}'_j$ is calculated based on Darcy's law for flow through porous media, as described in reference [7].

The diffusion term governs the transport of the generated CO_2 both inward and outward. The diffusion coefficient is evaluated at the interface between two adjacent shells, considering the effective diffusion coefficient $D_{eff,k}$ for the components $k = \{CaCO_3, CaO\}$ within the porous structure and the reaction progress [7].

The model has been validated in our previous paper [7] using experimental measurements for a single spherical particle.

2.6. DEM-CFD Coupling Routine

A one-way coupling approach is used for momentum exchange, meaning that while the particle bed influences the gas flow, the motion of the particles remains unaffected by drag or buoyancy forces. For the exchange of energy and species, a

two-way coupling method is applied, where fluid properties are transferred from the gas to the particles as boundary conditions and source terms are transferred from the solid phase to the fluid phase. More information on DEM-CFD coupling can be found in [13].

3. SIMULATION SETUP

The computational domain employed in this study is adapted from our previous work [8]. It consists of a box with dimensions 0.4 × 0.3 × 0.1 [m³], as illustrated in Figure 1, and is discretized into 6200 hexahedral elements. Mesh size in the bulk region is 0.02×0.02×0.02 [m³]. Finer mesh elements are applied in the upper section of the domain.

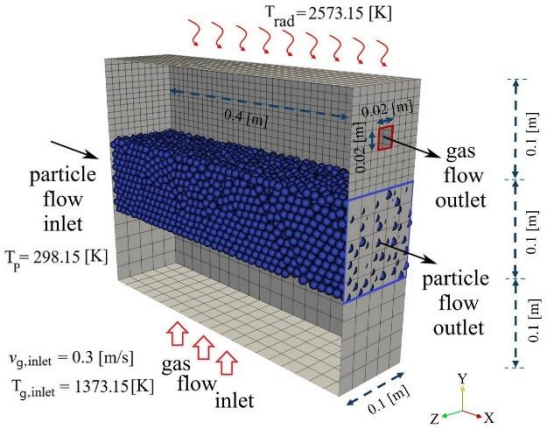

Figure 1. The meshed domain and boundary conditions. Reproduced from Abdi et al., 2025 [8], under CC BY 4.0

Air (comprising 23% O_2 and 77% N_2 by mass) enters the system through the bottom surface with a velocity of 0.3 m/s and temperature of 1373.15 K and exits via a small outlet (0.02 × 0.02 [m²], positioned at the top right boundary of the box), highlighted in red in Fig. 1. Particles flow through the left boundary (0.1 × 0.1 m) at 298.15 K and exit via the right outlet. The outlet boundary has a zero-gradient condition for both velocity and temperature, and the outlet pressure is set to atmospheric (zero relative gauge pressure). A no-slip condition is applied to all walls, which are assumed to be adiabatic with respect to convection. Additionally, the top wall is maintained at a fixed temperature of 2573.15 K (T_{rad}), while the remaining walls are kept at 298.15 K for radiation purposes. The absorption coefficient a_w and the emissivity of the top wall ε'_w are both 0.7, while for all other walls, the values are 1.

Three random particle arrangements—dilute (540-spheres), moderate (2560-spheres), and dense (5000-spheres)—were studied. The corresponding packing porosities within the particle zone (not for the entire box) are 93%, 66.5%, and 34.5% for the dilute, moderate, and dense cases, respectively. These values represent averages; in the fluid simulations, the local porosity in each computational cell is used.

The particle arrangements are created as follows: Initially, 5000 spheres are randomly introduced into the domain through a DEM simulation by dropping them from the top. To generate the moderate and dilute cases, approximately half and then another 2000 spheres are randomly removed, respectively. On average, each fluid cell contains 10, 5.12, and 1.08 spheres for the dense, moderate, and dilute cases.

Each case maintains similar particle velocities and residence times but differs in solid mass flow rates. For all cases, particles are assigned a constant velocity of 0.0002 m/s along the x-axis. Their trajectories are prescribed, meaning that the DEM mechanical motion equations are not solved—only the thermo-chemical behavior is computed. The residence time for a particle to travel from the left to the right boundary, $t_{residence}$, is 2000 seconds. The working fluid is air, with a thermal conductivity of 0.04 W/(m·K). Table 1 presents the general parameters used in the DEM-CFD simulations.

Table 1. Simulation parameters

parameter	unit	value
CFD time step	[s]	0.0002
DEM time step	[s]	0.001
gas absorption coefficient	[m^{-1}]	0
gas emissivity	[-]	0
gas inlet velocity	[m/s]	0.3
gas thermal conductivity	[W/m·K]	0.04
particle diameter	[mm]	10
particle emissivity	[-]	0.85
particle initial mass	[g]	1.413
particle Poisson's ratio	[-]	0.35
particles residence time	[s]	2000
particle velocity	[m/s]	0.0002
particle Young's modulus	[Pa]	1×10^9
$CaCO_3$ properties		
density (without pore)	[kg/m³]	2812
heat capacity	[J/kg K]	836.8
molar mass	[kg/mol]	0.1
porosity	[-]	0.04
solid conductivity	[W/mK]	2.26
specific surface area	[m²/ kg]	16000
tortuosity	[-]	1.4142
permeability	[m²]	5×10^{-15}
CaO properties		
density (without pore)	[kg/m³]	3310
heat capacity	[J/kg K]	753.1
molar mass	[kg/mol]	0.056
porosity	[-]	0.543
solid conductivity	[W/mK]	0.7
specific surface area	[m²/ kg]	7000
tortuosity	[-]	1.4142
permeability	[m²]	5×10^{-15}

4. RESULTS

4.1. Radiation Field

Figure 2 illustrates the distribution of incident radiation G within the domain in [W/m²]. Fig. 2a presents the results for cases without calcination, while Fig. 2b corresponds to cases with calcination.

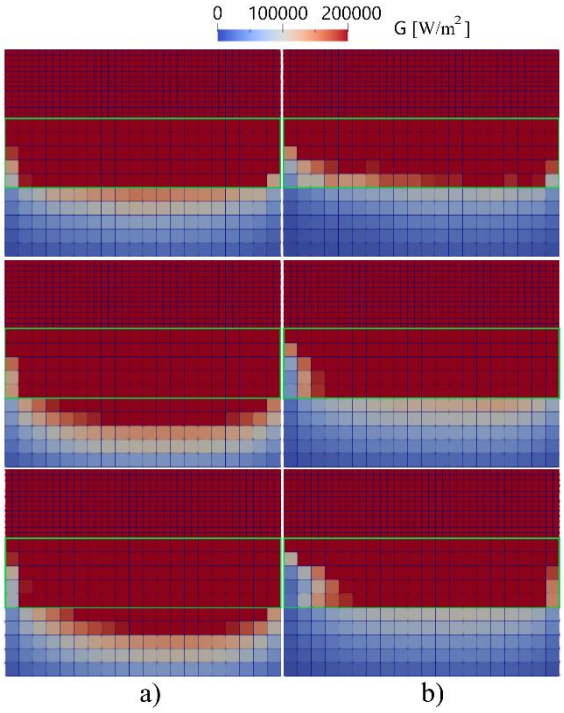

Figure 2: Incident radiation G [W/m²] contour in the case of 540 (top), 2560 (middle), and 5000 (bottom) spheres. a) without calcination. b) with calcination (G clipped above 200000 [W/m²]).

The local values of G indicate the extent to which radiation penetrates the particle bed. The particle-filled region is marked in green, so radiation reaches the lowest particle layer across all three packing densities. Notably, the radiation penetration depth is greater in the 2560- and 5000-sphere cases compared to the 540-sphere case. In the 2560 and 5000-sphere scenarios, the densely packed top layer absorbs more radiation from the upper wall. Over time, these top-layer particles emit more radiation toward the underlying layers, resulting in an increased radiation penetration depth.

As will be discussed in Figure 3, calcination causes a drop in particle temperature. Consequently, the top particle layers emit less radiation toward the lower layers, leading to a reduced radiation penetration depth. Therefore, the calcined cases exhibit lower values of G compared to the uncalcined cases.

4.2. Temperature Field

As the particles move through the system, they gradually absorb heat—primarily through convection from the bottom and radiation from the top. However, particles near the top layer, close to the outlet, are an exception—they are already heated due to high radiation absorption and lose heat via convection. Calcination begins as soon as the particle temperatures reach the threshold for this endothermic reaction which is around 800-900 °C.

According to Eqs. (15) and (18), the reaction rate of lime particles is governed by the local temperature and CO_2 mass fraction. In Fig. 3, the temperature field for both particles and fluid is shown for the two scenarios with and without consideration of calcination.

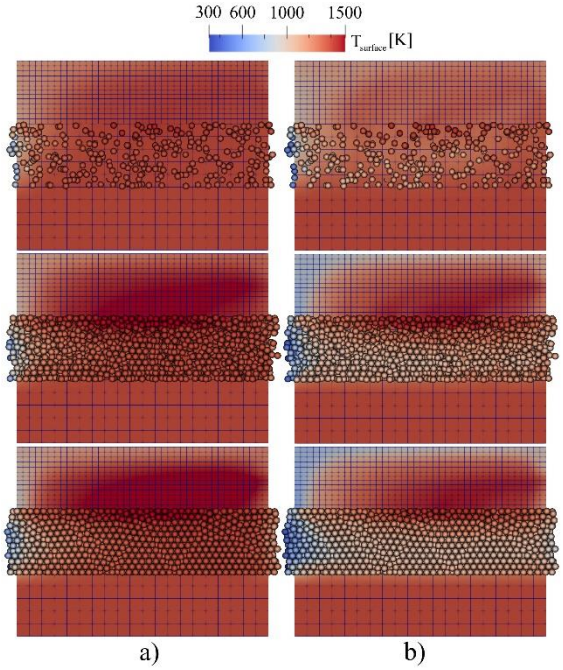

Figure 3: Surface temperature of particles in the case of 540 (top), 2560 (middle), and 5000 (bottom) spheres. a) without calcination. b) with calcination (clipped at 300 K and 1500 K).

The highest particle surface temperatures are observed in the upper region of the bulk, primarily due to radiation from the top. As expected, particle temperatures are slightly higher in the absence of calcination.

The maximum particle surface temperatures reach 1451 K, 1568 K, and 1568 K in the uncalcined cases. In the calcined cases, the maximum temperatures decrease to 1438 K, 1529 K, and 1503 K for the 540, 2560, and 5000 sphere cases, respectively. This difference is attributed to the temperature drop resulting from the endothermic nature of the calcination process. The temperature reduction occurs not only in regions with a high degree of calcination (see Figure 4a), but also

throughout the entire bulk region. This is because calcined particles at the top layers are colder than in the non-reacting case and therefore they emit less radiative heat to the lower layers.

Regarding the gas phase, the temperature above the bulk region is higher in the uncalcined case compared to the calcined cases. This is primarily because the hot particles at the top receive radiation heat from the top wall, and, without undergoing calcination, they retain more heat and transfer it to the gas through convection.

Radiation dominates heat transfer in all cases. In the calcined cases, average radiative transfer is 632 W, 3727 W, and 5922 W for the 540-, 2560-, and 5000-sphere cases, respectively, while convective transfer is lower at 360 W, 184 W, and 170 W. These are particle-averaged values; some particles gain heat by convection, others lose it.

4.3. Calcination Degree of the Lime Particles

Figure 4a shows the average calcination degree of lime particles across all radial shells for each case. The overall trends in the reacted particles are similar for all cases, with a high calcination degree observed near the upper section of the particle bed. This is primarily due to the radiation emitted by the hot top wall, which raises the particle temperatures significantly above the calcination threshold. Although the 540-particle case achieves a high overall calcination degree, some patches of uncalcined material remain, indicating non-uniform calcination. In fact, non-uniform calcination is observed across all three cases, with unreacted zones consistently appearing in the middle layers of the particle bed and near the particle inlet. This uneven calcination arises because particles in the middle layers receive neither sufficient radiation from the top wall nor adequate convective heat transfer from the bottom, preventing them from reaching the calcination temperature.

Notably, all three cases also show significant calcination at the lower part of the bed, attributed to the convective heat transfer from the incoming high temperature gas. Energy is transferred from the gas phase to supply the endothermic calcination reaction.

The key difference lies in the extent of the calcination zones: the 5000 case exhibits a smaller region with the highest calcination degree (red particles in Fig. 4a) compared to the 2560 case, which in turn shows a smaller high-calcination zone than the 540-sphere case. The simulation results yield average calcination degrees of 98%, 80%, and 60% for particles at the outlet in the dilute, moderate, and dense configurations, respectively, while the average calcination degrees for all particles are 65%, 48%, and 33%. These results demonstrate that the average calcination degree decreases with increasing packing density.

4.4. CO_2 Mass Fraction

Figure 4b illustrates the CO_2 mass fraction in both fluid and solid domain for each simulation case. Since the particles start with a uniform initial temperature of 298.15 K, there is no CO_2 production inside the particles at the inlet.

Particles gradually absorb heat, leading to the onset of calcination. Near the inlet, some top-layer particles appear red. As these particles move toward the outlet, they gradually change to orange and then blue as their internal CO_2 is released and transferred to the gas phase. Hence, the red top-layer particles in Fig. 4a have become orange (partially calcined particles) and blue (fully calcined particles with no remaining CO_2) in Fig. 4b.

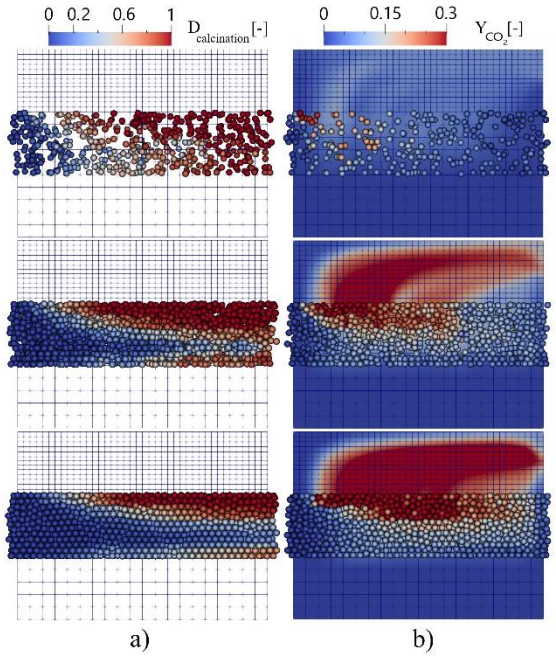

Figure 4: a) Calcination degree of lime particles b) Mass fraction of CO_2 (clipped to 0.3) in 540 (top), 2560 (middle), and 5000 (bottom) sphere cases.

Also, Fig. 4b shows the accumulation of CO_2 in the gas phase, resulting from the decomposition of limestone. Hence, the CO_2 concentration increases in alignment with the direction of the fluid flow. The amount of CO_2 in the fluid domain is highest in the 5000-sphere case due to the higher number of particles and, consequently, a greater amount of CO_2 released on the upper side of the bed. This is higher than in the 2560-sphere case, which in turn is higher than in the 540-sphere case. Therefore, although the overall calcination degree is lower in the 5000-sphere case, the influence of particle number is the dominant factor.

5. SUMMARY AND CONCLUSIONS

This study investigates the calcination behaviour of limestone particles, comparing results to cases where calcination is not considered. A Discrete Ordinates Method (DOM) is used in the coupled Discrete Element Method–Computational Fluid Dynamics (DEM-CFD) framework to model radiative heat transfer within systems of granular particles. The Averaged Volume Method was employed, introducing time-dependent source terms and a porosity field into the Navier-Stokes equations to account for the presence of particles. By incorporating local bed porosity in the modelling of particle emission and absorption, the effects of varying packing densities were captured.

A numerical test case has been simulated to analyse the interaction of heated walls, a moving particle bed with prescribed velocity, and a cross-flow of hot air. Spherical limestone particles were heated by a top wall at 2573.15 K and by cross-flowing air at 1373.15 K, with a constant inlet velocity of 0.3 m/s. Thermal conduction between particles has also been modelled. Three granular assemblies, with varying packing densities—dilute (93% porosity), moderate (66.5% porosity), and dense (34.5% porosity)—were considered, comprising 540, 2560, and 5000 particles, respectively. All scenarios shared the same residence time of 2000 seconds.

This work successfully demonstrates the influence of particle packing density and radiative heat transfer on the calcination process within moving particle beds. It was observed that as the particle number increased, the highest calcination degrees are concentrated in the upper and lower particle layers of the bed. Furthermore, the calcination degree distributions showed regions, particularly near the inlet and between densely packed lower and upper layers, where almost no calcination occurred. The average calcination degree decreases with increasing packing density. The simulation results yield average calcination degrees of 98%, 80%, and 60% for outlet particles in the dilute, moderate, and dense configurations, respectively.

Although the academic case studied here cannot be directly scaled to industrial kilns, the importance of granular packing, and radiation effects is highlighted.

ACKNOWLEDGEMENTS

This work has been funded by the Deutsche Forschungsgemeinschaft (DFG, German Research Foundation) – Project-ID 422037413 – TRR 287. Gefördert durch die Deutsche Forschungsgemeinschaft (DFG) – Projektnummer 422037413 – TRR 287.

REFERENCES

[1] Duan, S., Li, B., Rong, W. (2022a). Numerical simulation study of mixed particle size calcination processes in the calcination zone of a parallel flow regenerative lime kiln. *Materials*, 15(13), 4609.

[2] Abdi, R., Krzaczek, M., & Tejchman, J. (2023). Simulations of high-pressure fluid flow in a pre-cracked rock specimen composed of densely packed bonded spheres using a 3D CFD model and simplified 2D coupled CFD-DEM approach. *Powder Technol.*, 417, 118238.

[3] Abdi, R., Krzaczek, M., & Tejchman, J. (2022). Comparative study of high-pressure fluid flow in densely packed granules using a 3D CFD model in a continuous medium and a simplified 2D DEM-CFD approach. *Granul. Matter*, 24, 1-25.

[4] Krause, B., Liedmann, B., Wiese, J., Wirtz, S., & Scherer, V. (2015). Coupled three dimensional DEM-CFD simulation of a lime shaft kiln-calcination, particle movement and gas phase flow field. *Che. Eng. Sci.*, 134,834-849

[5] Kang, Z., et al. (2023). DEM-CFD coupled simulation of limestone calcination and fuel combustion in beam type lime shaft kiln. Applied Thermal Engineering, 231, 120935.

[6] Krause, B., & Liedmann, B., et al. (2017). 3d-dem-cfd simulation of heat and mass transfer, gas combustion and calcination in an intermittent operating lime shaft kiln. *Int. J. Therm. Sci.*, 117, 121-135

[7] Illana, E., Merten, H., et al. (2023). DEM/CFD simulations of a generic oxy-fuel kiln for lime production. *Therm. Sci. Eng. Prog.*, 45, 102076

[8] Abdi, R., Jaeger, B., et al. (2025). Modelling of heat transfer in moving granular assemblies with a focus on radiation using the discrete ordinate method: A DEM-CFD approach. *Particuology*, 100, 78-94.

[9]https://bulk-reaction.de/(accessed Apr. 11, 2025).

[10]https://www.openfoam.com/documentation/guides/v2012/doc/. (accessed Apr. 11, 2025).

[11] S. Ergun, A.A. Orning, Fluid flow through randomly packed columns and fluidized beds, *Ind. Eng. Chem*. 41 (6) (1949) 1179–1184.

[12] Hilse, N., Kriegeskorte, M., et al. (2023). Discrete Element Simulations of Contact Heat Transfer on a Batch-Operated Single Floor of a Multiple Hearth Furnace. *Processes*, 11(12), 3257.

[13] Illana Mahiques, et al. (2023). Locally resolved simulation of gas mixing and combustion inside static and moving particle assemblies. *Che. Eng. & Tech.*, 46(7), 1362-1372.